Time-resolved surface photovoltage measurements at *n*-type photovoltaic surfaces: Si(111) and ZnO(10$\bar{1}$0)

Ben F. Spencer,[1,2,*] Darren M. Graham,[1,2] Samantha J. O. Hardman,[1,†] Elaine A. Seddon,[1,2] Matthew J. Cliffe,[1,2] Karen L. Syres,[1,‡] Andrew G. Thomas,[1] Stuart K. Stubbs,[1,§] Fausto Sirotti,[3] Mathieu G. Silly,[3] Paul F. Kirkham,[1,§] Asurasinghe R. Kumarasinghe,[1,‖] Graeme J. Hirst,[4] Andrew J. Moss,[2] Stephen F. Hill,[2] David A. Shaw,[2] Swapan Chattopadhyay,[1,2,5] and Wendy R. Flavell[1]

[1]*School of Physics and Astronomy and the Photon Science Institute, The University of Manchester, Manchester M13 9PL, United Kingdom*
[2]*The Cockcroft Institute, Sci-Tech Daresbury, Keckwick Lane, Daresbury, Warrington WA4 4AD, Cheshire, United Kingdom*
[3]*Synchrotron-SOLEIL, BP 48, Saint-Aubin, F91192 Gif sur Yvette CEDEX, France*
[4]*STFC Rutherford Appleton Laboratory, Didcot OX11 0QX, United Kingdom*
[5]*Department of Physics, The University of Liverpool, Liverpool L69 7ZE, United Kingdom*

(Received 5 March 2013; revised manuscript received 7 October 2013; published 4 November 2013)

The time-resolved change in the surface potential upon photoexcitation has been measured in two *n*-type photovoltaics, Si (111) 7×7 and ZnO (10$\bar{1}$0), using two different laser pump-synchrotron x-ray probe methodologies. Taken together, these experiments allow the dynamics of the surface photovoltage (SPV) to be monitored over timescales of subnanoseconds to milliseconds. The timescales for the photoinduced change in the SPV are dramatically different in the two samples, with measured SPV decay time constants of 6.6 μs for Si and up to 1.2 ms (dependent on surface oxygen concentration) for ZnO. The carrier dynamics at the Si (111) 7×7 surface are well modeled by a self-decelerating relaxation model involving the recombination of carriers by thermionic emission across the surface depletion layer on nanosecond timescales. In the case of ZnO (10$\bar{1}$0), a persistent photoconductivity (PPC) is observed, which is influenced by oxygen annealing conditions during sample preparation. Persistent photoconductivity is also observed when the surface is illuminated with subband-gap (405 nm) radiation, revealing that defect states approximately 340 meV above the valence band edge are directly associated with the PPC. We demonstrate that, under the conditions of our experiment, PPC mediated by these defects dominates over the oxygen photodesorption mechanism. These observations are consistent with the hypothesis that ionized oxygen vacancy states are responsible for PPC in ZnO.

DOI: 10.1103/PhysRevB.88.195301 PACS number(s): 68.47.Fg, 68.35.Ja, 73.25.+i, 72.20.−i

I. INTRODUCTION

Silicon remains the most important material used in photovoltaic (PV) applications, having been used to fabricate solar cells since the 1940s[1] and accounting for 90% of commercially available devices as of 2008.[2] However, there is an urgent need to lower the cost of solar energy, and this has led to a widespread search for new PV technologies and alternative photoanode and photocathode materials.[3,4] An important property of one of the electrodes of any solar device is transparency, leading to a new focus on transparent conducting oxides or TCOs.[3,5–9] Our understanding of carrier dynamics in these materials is in its infancy and has motivated this study, where we compare the photoexcited carrier dynamics in the archetypal photovoltaic Si [using the Si (111) 7×7 surface], with those at the surface of a potential next-generation photoanode material, the TCO ZnO[3,7,10–13] [using the nonpolar *m* plane (10$\bar{1}$0) surface].

The two photovoltaics studied here are chosen to have formally similar surface electronic structure; both are *n* type, with surface states which in a conventional semiconductor are expected to give rise to upward band bending and an electron depletion layer at the surface as shown in Fig. 1.[14] In the case of the well-studied Si (111) 7×7 reconstruction, the position of the Fermi energy at the surface is pinned by a half-filled surface state,[15] which effectively forms a Schottky barrier at the surface. The binding energies of the different surface sites have been well characterized by x-ray photoelectron spectroscopy (XPS),[16,17] and the system thus provides a good benchmark for studies of less well-characterized systems.

The band gap of ZnO (∼3.4 eV)[3,7,18] is significantly larger than that of Si (around 1.1 eV).[19] It is intrinsically nonstoichiometric, naturally exhibiting *n*-type behavior, but despite its use as a gas sensor material for decades,[7] its defect chemistry remains a topic of controversy.[3,20,21] It was initially assumed that *n*-type doping arose from the presence of oxygen vacancies V_O, and it seems undoubtedly the case that such vacancies are present[3,7,20,21] (together with other defects, including Zn interstitials, Zn vacancies, and defect complexes).[3,7,20] However, recent work has emphasized the importance of hydrogen as a donor in ZnO, giving *n*-type conductivity that depends on the concentration of oxygen vacancies, $[V_O]$, as the hydrogen donors occupy the oxygen sites H_O.[22,23] Similarly, the origin of persistent photoconductivity (PPC) in ZnO (where photoconductivity persists after the exciting source has been switched off) continues to be extensively debated.[3] Persistent photoconductivity in ZnO has for some years been attributed to hole capture from the surface depletion layer by chemisorbed O_2^-,[24–30] and the oxygen environment has been shown to influence the lifetime of PPC.[9,31] However, more recent work has emphasized the importance of oxygen vacancies; modeling results have suggested that PPC is controlled by band-gap states associated with metastable doubly[21,32,33] or singly charged[34] oxygen vacancies, which are also thought to be responsible for the green defect (GD) luminescence of ZnO.[33–36] Persistent photoconductivity has

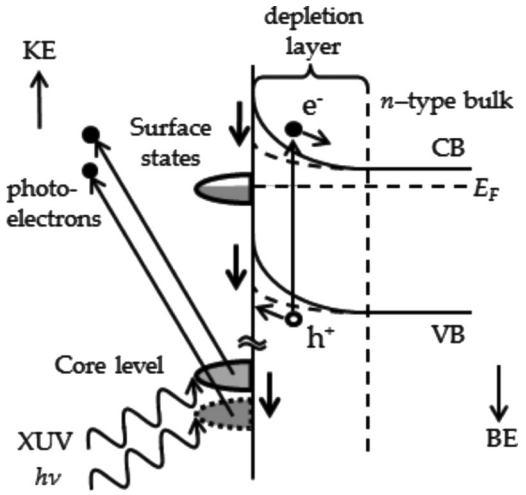

FIG. 1. Nonequilibrium SPV in a conventional n-type semiconductor probed using XPS. Laser illumination promotes electrons (e^-) across the band gap from the VB to the CB, which then migrate into the bulk material due to the presence of the depletion layer. The corresponding holes (h^+) migrate to the surface. The electric field within the space charge region and hence the band bending are reduced (dashed lines). The BE of the core electron energy levels are thus increased, reducing the kinetic energy (KE) of photoelectrons liberated upon x-ray absorption. Here, E_F denotes the position of the Fermi level prior to photoexcitation, which is pinned by the surface states.

been associated with the loss of lattice oxygen[29,31] and also with H_2 molecules trapped at oxygen vacancy sites.[37] The assumption of a depletion layer at the surface of n-type ZnO is also open to question, as a series of elegant experiments on the surfaces of n-type TCOs such as CdO, ZnO, In_2O_3 $SrTiO_3$, and SnO_2 have shown that, at sufficiently low doping levels, the surfaces can show accumulation rather than depletion layers.[3,38,39] Such observations prompt an examination of the charge dynamics at the surfaces of n-type photoanode materials like ZnO, and indeed the need for such measurements has been noted.[40]

These may be probed through the surface potential change on photoexcitation. Upon photoexcitation, in the presence of a surface depletion layer, electrons are promoted into the conduction band (CB) of the semiconductor and migrate into the bulk, reducing the amount of band bending at the surface (Fig. 1), and it is this illumination-induced change in the surface potential that is known as the surface photovoltage (SPV) effect.[41,42] The effect may be observed in photoemission experiments, especially at low temperature where electron-hole pair recombination rates are low.[43] It may also be induced by illuminating the surface with laser radiation of energy sufficient to promote electrons across the band gap; use of a pulsed laser then allows the time dependence of the SPV, and hence the nonequilibrium band bending at the semiconductor surface, to be probed.

A suitable time-resolved experiment to measure the nonequilibrium SPV uses a laser-pump x-ray-probe arrangement where a laser, used to photoexcite the sample, is synchronized to an x-ray source such as that from a synchrotron facility, so that the pump-probe delay time can be varied. X-ray photoelectron spectroscopy is used to probe the sample at a range of delay times after the laser pump beam has photoexcited the sample. The experiment measures the change in SPV (which we term the SPV shift ΔV_{SP}) induced by the laser illumination (Fig. 1), i.e., the change in the surface potential induced by the additional photocarriers generated by the laser pulse (over and above any SPV induced by the photoemission process itself).[14]

Surface photovoltage measurements have been made on a variety of Si and other semiconductor surfaces using both optical[44–54] and free-electron laser pump beams[55,56] and a variety of experimental configurations; some of these experiments have been recently reviewed by Yamamoto *et al.*[57] For example, Widdra *et al.*[48] and Bröcker *et al.*[49] utilized the single-bunch mode of the BESSY synchrotron to provide a time window of 800 ns in studies of the SiO_2/Si (100) interface. Experiments carried out by us at the UK Synchrotron Radiation Source (SRS) followed this approach by synchronizing a laser system to the synchrotron in single-bunch mode, giving a time window of 320 ns (see Sec. II A).

Here, we use laser-synchrotron pump-probe spectroscopy to examine the carrier dynamics at the ZnO m-plane ($10\bar{1}0$) surface and contrast them with those observed for the conventional semiconductor surface, Si (111) 7×7, under similar conditions. By combining data accumulated in two different pump-probe modes, we are able to access timescales from subnanoseconds to milliseconds and longer. We find that the carrier dynamics at the Si (111) 7×7 surface are well modeled by the recombination of carriers by thermionic emission across the surface depletion layer on nanosecond timescales. We obtain a consistent value for the dark carrier lifetime by removing the background due to preceding pulses from the SPV transient and discuss the effect of this background on our data. Under the conditions of our experiment (which require a relatively high intrinsic donor concentration), we observe SPV shifts at the ZnO surface consistent with the presence of a depletion rather than an accumulation layer. Our results demonstrate a persistent oxygen-mediated photoconductivity in ZnO. We show that, under the conditions of our experiment, PPC is governed by the oxygen vacancy concentration, and this dominates over the oxygen photodesorption mechanism. This conclusion is supported by the observation of similar dynamics in experiments conducted using subband-gap energy excitation, revealing that defect states above the valence band (VB) edge are directly associated with the PPC. These observations are consistent with the hypothesis that ionized oxygen vacancy states are responsible for PPC in ZnO.[32] We discuss the consequences for the application of ZnO as a transparent photoanode. Despite the different timescales of the SPV decay in these two photovoltaics, we find that both cases are appropriately treated by a model in which the SPV shift self-decelerates,[48,49] allowing us to adopt a consistent framework for extraction of carrier lifetimes.

II. EXPERIMENTAL

A. Pump-probe measurements

Laser-synchrotron pump-probe measurements were carried out at two synchrotron sources, the SRS at Daresbury, UK,

and SOLEIL, Saint-Aubin, France. At the SRS, a Ti:sapphire ultrafast oscillator (Spectra-Physics, Tsunami) was synchronized to a divided-down reference frequency from the 499.68 MHz SRS master clock using a commercial phase-lock loop electronics module (Spectra-Physics, Lok-to-Clock). The SRS was run in a single-bunch mode of operation, where only one of the 160 available rf buckets was filled with electrons, resulting in one electron bunch [of maximum pulse duration 200 ps full width at half-maximum (FWHM) height][58] orbiting at a repetition rate of 3.123 MHz. To obtain the same repetition rate from the oscillator, it was necessary to use an acousto-optic modulator-based pulse picker (Angewandte Physik & Elektronik) to select every 26th pulse from the 81.198 MHz laser pulse train. This resulted in pairs of x-ray and laser pulses being delivered to the sample position every 320 ns. The use of a photodiode sensitive to both soft x-ray and infrared radiation (International Radiation Detectors, model AXUVHS1)[59] enabled spatial and temporal overlap to be achieved at the sample position, with the laser spot size (3 mm^2) completely eclipsing the x-ray beam (of profile $\sim$2 mm horizontally $\times$ 0.1 mm vertically). This is necessary to ensure that the x-ray beam probes only the region of the sample pumped by the laser. The r.m.s. timing jitter between the laser and synchrotron radiation (SR) pulses was measured to be approximately 25 ps by using the photodiode to take repeated measurements of the two pulses. To vary the delay time between the laser pump pulse and x-ray probe pulse a digital phase shifter (Analog Devices, direct digital synthesizer, model AD9959/PCB) was used to adjust the phase of the reference frequency supplied to the oscillator. Measurements of the transient SPV on Si (111) used the 800 nm (1.55 eV) Ti:sapphire output, producing 90 fs pulses with a fluence of 58 nJ cm^{-2} at the sample surface and a synchrotron photon energy of 140 eV (chosen to maximize surface sensitivity without undue loss of flux). Experiments on ZnO ($10\bar{1}0$) required the oscillator output to be tuned to 720 nm and frequency doubled to provide 360 nm (3.44 eV) due to the larger band gap of ZnO. X-ray photoelectron spectroscopy was carried out using a SCIENTA SES2000 analyzer, probing the Si 2p and Zn 3d core levels in order to measure the laser-induced SPV. The overall experimental (monochromator + analyzer) resolution was 0.25 eV, and the position of the Fermi energy was measured using a metal in contact with the sample. Careful checks were made to ensure that sample charging under either the x-ray or laser beam was eliminated. For each time delay setting, a spectrum was recorded without laser illumination both before and after the photoexcited spectrum, in order to ensure that the spectrum returned exactly to its original binding energy (BE) position. This allowed the SPV shift to be measured across a 320 ns time window with a subnanosecond time resolution limited by the 200 ps pulse duration of the synchrotron.[58]

Time-resolved XPS measurements were also carried out under laser illumination on the TEMPO beamline at Synchrotron-SOLEIL.[60] Here, a continuous wave (CW) 10 mW laser (Coherent, CUBE) operating at 372 nm was modulated using a square-wave signal from a pulse generator, typically switching the laser pump beam on every 0.5 ms (i.e., a repetition rate of 2 kHz), with a maximum fluence of $\sim$25 μJ cm^{-2}. The pulse generator was also used to trigger in-house software recording an XPS spectrum over a narrow BE range every 50 ns. These spectra were recorded using a SCIENTA SES 2002 analyzer with a two-dimensional (2D) delay-line detector.[61,62] The time resolution was determined to be approximately 150 ns, limited by the time difference in the signals from the delay-line detector and the speed of the electronics. Data were typically recorded across a time window of a few milliseconds. In excess of 10 000 accumulations were required to achieve satisfactory signal-to-noise ratios. Spatial overlap of the x-ray beam (measuring $\sim$150 μm vertically $\times$ 100 μm horizontally) and the laser beam at the sample was achieved using a charge-coupled device (CCD) camera. A photon energy of 140 eV was used, and the typical experimental (monochromator + analyzer) resolution was 150 meV. Care was again taken to check for and eliminate sample charging as described above.

These two experimental arrangements taken together allow measurement of the pump-induced SPV changes over a very wide range of timescales, from subnanoseconds to milliseconds and longer. While the former is suitable to probe the carrier dynamics of a semiconductor such as Si, the latter was found to be necessary to probe SPV transients in ZnO.

B. Sample preparation

The n-type phosphorus-doped silicon (111) wafer used in this study was manufactured by Siltronix. The wafer had a thickness of 0.5 mm and a resistivity of 5 ± 2 Ω cm, corresponding to a doping level of approximately 10^{15} cm^{-3}. The surface was prepared under ultrahigh vacuum (UHV) conditions by annealing using an electron beam. The surface was first outgassed at 1073 K for several hours prior to repeated flashing to 1273 K, to produce the well-known 7×7 surface reconstruction.[63,64]

The m-plane ZnO ($10\bar{1}0$) surface was prepared using an established recipe.[65–69] The surface n-type conductivity of ZnO may be enhanced in UHV by sputtering, a process that creates donors such as oxygen vacancies at the surface[70–72] (possibly together with other defects and defect complexes with oxygen vacancies).[3,7,66] Careful sample preparation is required to enhance the surface concentration of these vacancies in order to avoid sample charging in photoemission. The sample underwent three repeated cycles of argon ion sputtering and electron beam annealing, up to a temperature of 1023–1043 K. Following this, the sample was then annealed in $1.2–1.4 \times 10^{-7}$ mbar oxygen at 703 K in order to heal some of the excess oxygen vacancies created by sputtering at the surface.[66] This step is important in controlling the final conductivity of the surface. In order to explore the effect of oxygen vacancy concentration on the dynamics, the annealing period was varied between 10 and 20 min, creating different oxygen vacancy (and hence donor) concentrations[73] in the near-surface layers.[74–76] The sample was then allowed to cool in the presence of oxygen, before a low-temperature anneal (603 K, 20 min), followed by a short high-temperature anneal *in vacuo* (1023–1043 K, 10 min),[77] completing the cleaning process. A final high-temperature flash anneal *in vacuo* has previously been used to remove residual adsorbed oxygen;[77] here, it was found to be necessary to eliminate charging during the pump-probe experiment (Sec. IV B).

The surfaces were diagnosed as uncontaminated using low-energy electron diffraction, where sharp Si (111) 7×7 and ZnO $(10\bar{1}0)$ 1×1 patterns were obtained,[68] and XPS showing no C 1*s* signal. Measurements were carried out at room temperature at pressures in the range $1–8 \times 10^{-10}$ mbar.

III. SPV THEORY

The amount of band bending at a semiconductor surface changes under photoexcitation. The total change in the band bending at the surface, or SPV ΔV_{SP}^{tot}, upon illumination is described by:[14]

$$\frac{\Delta V_{SP}^{tot}}{kT}\exp\left(\frac{\Delta V_{SP}^{tot}}{kT}\right) = \frac{n_P}{n_0}\exp\left(\frac{V_0}{kT}\right). \quad (1)$$

Here, n_0 is the doping carrier concentration, n_P is the photoexcited carrier concentration, and V_0 is the equilibrium band bending. In our experiment, where we measure the change in SPV ΔV_{SP} induced by the laser illumination, the photoexcited carrier concentration is determined using the laser fluence, energy, and absorption coefficient. A change in the surface potential also affects the photoexcited carrier lifetime τ,[48]

$$\tau = \tau_\infty \exp\left(\frac{-\Delta V_{SP}}{\alpha kT}\right), \quad (2)$$

where α is a material parameter (typically with values ranging from 0.5 to 2)[49] and τ_∞ is the dark carrier lifetime (the lifetime of carriers in the absence of a SPV). The parameter α is likened to the ideality factor in a Schottky diode.[42] A theoretical study by Schulz *et al.*[78] on *p*-type silicon (with a doping level of 10^{15} cm^{-3}) showed that values for α were consistently less than 1 and that the parameter also correlated with the equilibrium band bending V_0 (values for α of 0.73, 0.78, and 0.89 were obtained for V_0 values of 0.25, 0.39, and 0.65 eV, respectively).

After photoexcitation, the recombination rate is assumed to be limited by the process of overcoming the barrier induced by the band bending by thermionic emission across the depletion layer.[48] The SPV shift reduces in a dynamic way as recombination occurs [Eq. (1)], and thus the photoexcited carrier lifetime increases with time [Eq. (2)] as the surface potential returns to equilibrium. The decay of the SPV after the laser is switched off is thus modeled as a constant deceleration, as developed in Widdra *et al.*[48] and Bröcker *et al.*[49] For the $\Delta V_{SP}^{tot} > kT$ case, the decay of the SPV shift over time $\Delta V_{SP}(t)$ can be described by:[48]

$$\Delta V_{SP}(t) = -\alpha kT \ln\left[\exp\left(\frac{-\Delta V_{SP}^{tot}}{\alpha kT}\right) + \frac{t}{\tau_\infty}\right]. \quad (3)$$

For the case where $\Delta V_{SP}^{tot} \sim kT$, a more general form has been proposed:[49]

$$\Delta V_{SP}(t) = -\alpha kT \ln\left\{1 - \exp\left(\frac{-t}{\tau_\infty}\right)\left[1 - \exp\left(\frac{-\Delta V_{SP}^{tot}}{\alpha kT}\right)\right]\right\}. \quad (4)$$

The onset of the pump-induced SPV change when the laser is switched on may be modeled by a single exponential if the rate of carrier creation far exceeds recombination (i.e., at sufficiently high fluence).[42] Otherwise, a biexponential or a decelerated exponential model analogous to Eq. (4) may be appropriate. The latter reflects the dynamic increase in recombination rate as the surface band bending is reduced, which acts to counterbalance the rate of carrier creation.

In this model, the pump-induced change in the surface band bending is logarithmically dependent on the number of induced charge carriers [Eq. (1)] and hence the photoexcitation fluence Φ,

$$\Delta V_{SP}^{tot}(\Phi) = \alpha kT \ln(1 + \gamma\Phi), \quad (5)$$

where γ is another material parameter.[49]

IV. RESULTS

A. The Si (111) 7 x 7 surface

The SPV shift at the Si (111) 7×7 surface upon photoexcitation with an 800 nm pump beam was measured using XPS of the Si 2*p* core level at a BE of approximately 99 eV. Typical spectra are shown in Fig. 2. In the absence of photoexcitation, the Si 2*p* core level signal shows a two-peaked structure with a FWHM of approximately 1.2 eV, and a peak maximum at 99.1 eV BE. This is due to a number of surface and bulk components, discussed further below. The laser-induced shift in the BE of this core level (due to a change in the surface band bending) can be seen in Fig. 2, where a shift in the BE of the core-level energy spectrum of approximately $+0.4$ eV is seen at a pump-probe delay time of 4 ns. A shift to higher BE is expected for an *n*-type semiconductor as illustrated in Fig. 1. [In separate experiments using a *p*-type Si (111) substrate with an accumulation layer at the surface, a SPV shift to lower BE was obtained, as expected (Appendix A, Fig. 10)]. Core-level spectra recorded without photoexcitation before and after each spectrum taken with laser illumination were found to overlie

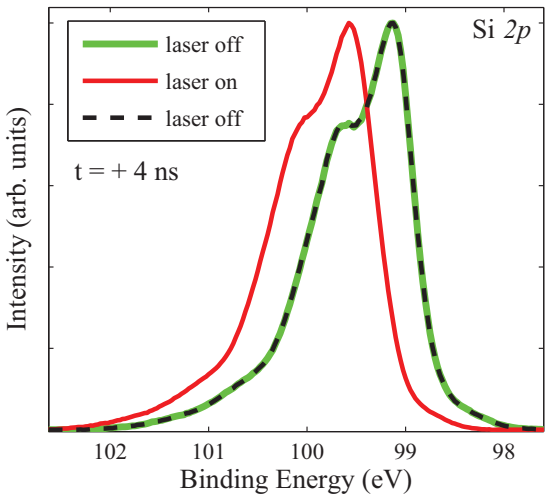

FIG. 2. (Color online) The Si 2*p* core level spectrum of the Si (111) 7×7 surface, obtained using a photon energy of 140 eV. The spectrum is shifted to higher BE when photoexcited with an 800 nm pump beam (at a fluence of 58 nJ cm^{-2}) at a pump-probe delay time of 4 ns before the x-ray probe. Spectra without laser photoexcitation taken before (green line) and after (black dashed line) the laser-on spectrum show that the peak returns to its original BE after photoexcitation (the spectra overlie each other).

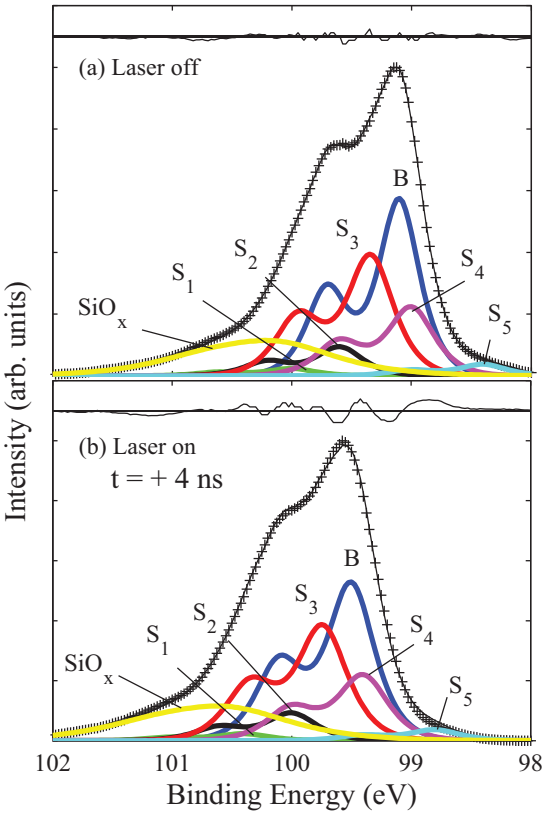

FIG. 3. (Color online) Peak fitting of the Si $2p$ core-level spectra shown in Fig. 2, (a) without and (b) with laser photoexcitation. The XPS data are shown as crosses and the combined fit is shown with a line through these data. The bulk (B) and surface (S_1, etc.) state fits follow the parameters outlined by Le Lay *et al.* (see text).[16] A magnified residual is shown above each figure.

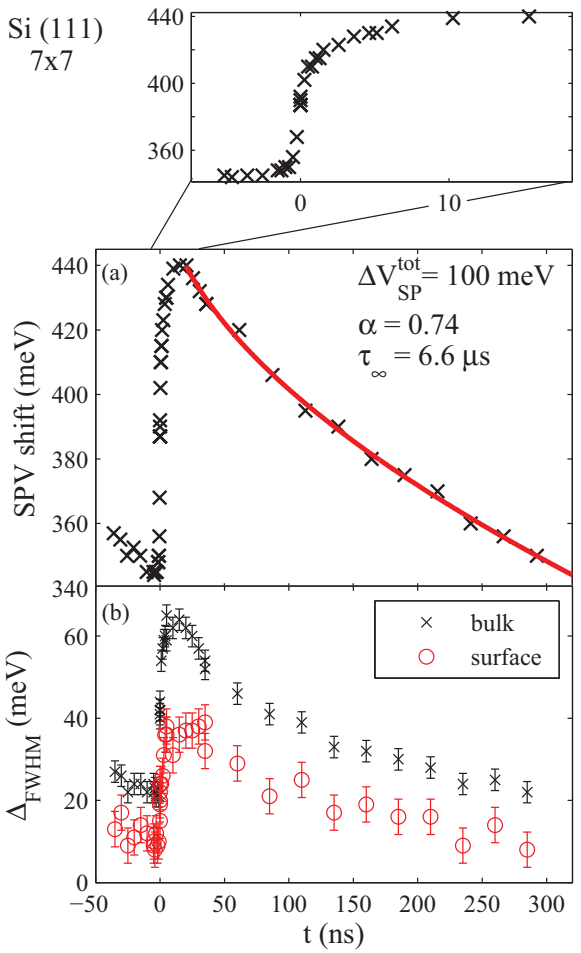

FIG. 4. (Color online) (a) The pump-induced change in the SPV for an n-type Si (111) 7×7 surface, excited with 800 nm radiation. The decay is fitted using the multiple-pulse model of Eq. (B2), giving a dark carrier lifetime of 6.6 μs. The inset shows the rising edge of the pump-induced SPV change. (b) The increase in FWHM, Δ_{FWHM}, of the surface and bulk components (relative to their values in the absence of the pump) as a function of pump-probe delay time.

each other (Fig. 2 and Appendix A, Fig. 10), confirming the absence of residual sample charging.

The Si $2p$ core level spectrum of the Si (111) 7×7 surface is well characterized, and we follow the peak fitting parameters established by Le Lay *et al.*[16] Figure 3 shows the components fitted to the spectra, both with and without laser photoexcitation (marked "laser on" and "laser off"). The $2p_{3/2,1/2}$ doublet separation was fixed at 0.605 eV, and the separate components were fitted using sum approximation Voigt functions[79] (70% Lorentzian) with CasaXPS.[80] The spectral components include a bulk component (B) along with various surface state components (S_1–S_5). These have been extensively discussed and assigned by others.[16,63,64] The BE positions and relative intensities of these states are in good agreement with Le Lay *et al.*[16] A broad tail at higher binding energies in Figs. 3(a) and 3(b), fitted by a component labeled SiO_x, is attributed to a range of oxidized states that were not completely removed during cleaning.[81,82] This is fitted as a broad (FWHM $>$ 1 eV) component.

Upon laser photoexcitation, the core-level energy spectrum is broadened. In order to fit the spectra, we assume that the population of these states does not change on photoexcitation.[83] The bulk and surface states without laser photoexcitation have FWHMs of 0.40 and 0.45 eV, respectively. During laser photoexcitation, as shown in Fig. 3, the bulk component broadens to have a FWHM of 0.46 eV, and the surface states to a FWHM of 0.49 eV. A study by Marsi *et al.*[84] on the Si (111) 2×1 surface found similar broadenings of the Si $2p$ spectrum, with a SPV shift (160 meV) comparable to this study. This broadening is discussed further below.

The BE shift seen in the Si $2p$ core level spectrum was measured at different pump-probe delay times (Fig. 4). For time delays of 20–300 ns, we observe a nonexponential decay of the SPV over a timescale of several hundred nanoseconds, consistent with the observations of Widdra *et al.*[48] for the SiO_2/Si (100) interface. In Fig. 4, the SPV shift lies on a time-varying background of approximately 345–300 meV, which is attributed to the residual SPV induced by preceding laser pump pulses, which photoexcite the sample every 320 ns (i.e., the band bending does not return to its equilibrium value within the 320 ns time window provided by the repetition rate of the synchrotron). Therefore, to fit the data according to Eq. (3), removal of the background due to these preceding pump pulses is required. We adopt the procedure given in Appendix B. Increasing the number of preceding

pump pulses in the model leads to a convergence of the fitting parameters when all the preceding pulses that can influence the SPV decay have been included (see Appendix B, Fig. 11). Convergence of the fit is achieved after 20 previous photoexcitations are included in the model (as shown in Fig. 11), i.e., a photoexcitation equilibrium is reached after 21 laser photoexcitations. A change in the surface potential of 100 meV with each photoexcitation pulse is obtained from this fitting procedure, together with a dark carrier lifetime τ_∞ of 6.6 μs and a material parameter α of 0.74.

The dark carrier lifetime is consistent with literature values. Ogawa *et al.* [52] find a relaxation time of 0.5 μs for a Si (111) 7×7 surface with a resistivity of 0.01 Ω cm, and Hamers and Cahill[85] obtain a relaxation time of 1 μs for a p-type Si (111) 7×7 sample with a resistivity of 0.1 Ω cm. The resistivity of the sample used here was $\sim$5 Ω cm, with a fitted dark carrier lifetime of 6.6 μs, consistent with the established increase in carrier lifetime with resistivity in Si.[85] However, Long *et al.*[44] report a relaxation time of 14 μs for n-type Si (111) 7×7, where the doping level was 1.1×10^{16} P (equivalent to a resistivity of $\sim$0.5 Ω cm). The apparent discrepancy in the measured carrier lifetimes with doping level is reconciled by noting the differences in the excess carrier concentration created upon laser illumination. Meier *et al.*[86] show that, while carrier lifetime decreases as the doping level increases, for Si, lifetimes increase as the excess carrier concentration increases (up to approximately 10^{17} cm^{-3} for doping levels of 10^{15} cm^{-3} and above). The laser fluence used in these experiments was 58 nJ cm^{-2}, whereas the work by Long *et al.*[44] used a laser fluence of 100 μJ cm^{-2}, three orders of magnitude larger. The extracted carrier lifetime of 6.6 μs is consistent with Meier *et al.*[86] for the doping level of $\sim 10^{15}$ cm^{-3} assuming an excess carrier concentration of $\sim 10^{14}$ cm^{-3} is created in our experiment. The lifetime of 14 μs measured by Long *et al.*[44] is also consistent with Meier *et al.*[86] if an excess carrier concentration of $\sim 10^{17}$ cm^{-3} is assumed, three orders of magnitude greater than that created in our experiment and consistent with the difference in fluence.

The slow onset of the pump-induced SPV [inset of Fig. 4(a)] at short time delays (up to 20 ns) limits the conclusions we can reliably draw about this time period. The full reasons for this slow onset are not completely clear; the timescales involved are far in excess of the timing jitter in the experiment ($\sim$25 ps). However, the width is influenced by a number of experimental factors, including the effect of the changing surface potential on electrons that have already left the sample when the photoexcitation pulse arrives, as described in detail by Widdra *et al.*,[48] which produces a broadening of around 1 ns. The shape of the onset is also affected by the residual SPV induced by preceding laser pump pulses (discussed above). The effect is to broaden the SPV maximum somewhat (as shown in Fig. 12, Appendix B). We observe no fast (a few hundred picoseconds to a few nanoseconds) component, consistent with the observations of Widdra *et al.*,[48] but in contrast with those of Ogawa *et al.* [52] and Marsi *et al.* [56] for the Si (111) 7×7 and 2×1 surfaces, respectively. The observation of the latter might indicate the presence of a fast decay channel mediated by surface states.[56] Its absence here suggests that the data are appropriately fitted using the self-decelerating charge relaxation model where the carrier lifetime increases as the SPV shift decays.[48,49] The significant differences in the onset data observed by different groups[48,52,56] merit further investigation.

Figure 4(b) shows the change in the FWHM of the surface and bulk components of the Si $2p$ photoelectron spectra as a function of pump-probe delay time. The broadening decreases as the pump-probe delay time increases and a lower amount of broadening is observed for the surface components. At the laser fluence used in our experiments, we estimate the temperature rise due to laser heating is significantly less than 1 K. Thus, this broadening cannot be associated with laser heating. Peak broadening during laser-SR SPV measurements has been observed previously and assigned to temporal averaging of rapid SPV variations during the synchrotron probe pulse.[84] However, we note that this mechanism would only give rise to a significant effect at short time delays where the SPV is changing rapidly; our measurements at long time delays show that the observed broadening must be due to another mechanism. The broadening is likely to be associated with the Gaussian profile of the laser pump beam, which creates more carriers at the center of the beam than at the edges. Thus, the SPV may vary with position across the pump beam and hence also across the relatively large probe beam that is coincident with it. This would broaden all the spectra taken under laser illumination, by an amount dependent on the size of the SPV at the time delay sampled as we observe [Fig. 4(b)]; the effect would be smaller for the surface states whose energies are effectively pinned by the Fermi energy, also as observed.

The equilibrium band bending V_0 obtained using Eq. (1) for a SPV of 100 meV is 0.21 eV. This places the Fermi level 0.64 eV above the VB maximum at the surface, as discussed in Appendix C and shown in Fig. 13. This value agrees well with other studies that show that the Fermi level is pinned between 0.63 and 0.65 eV above the VB maximum for this silicon surface.[44,87,88] The material parameter α is correlated with the value of V_0; the value obtained for α (0.74) for $V_0 = 0.21$ eV matches well with the value of $\alpha = 0.73$ for $V_0 = 0.25$ eV calculated for p-type silicon with the same doping level.[78] The observed maximum change in the surface potential ΔV_{SP}^{tot} of 100 meV indicates that the photoexcitation fluence used was not sufficient to fully remove the equilibrium band bending.

In our experiment, the 800 nm (1.55 eV) pump beam can excite electrons into the unoccupied (U_1) surface states of the Si (111) 7×7 surface,[15] (illustrated in Appendix C, Fig. 13) as well as across the band gap. The relaxation time for electron decay from the U_1 state into the bulk has been measured [using a very high photon fluence of 0.8 mJ cm^{-2} in two-photon photoemission (2PPE)] to be 140 ps.[15] This is at the limit of the time resolution available to us and is very unlikely to be observed at the low fluence (58 nJ cm^{-2}) of our experiment. We conclude that the primary process influencing the data of Fig. 4 is the recombination of carriers excited across the band gap of Si and that the data may be fitted by the self-decelerating charge relaxation model.[48,49]

B. ZnO ($10\bar{1}0$)

Similar laser-SR pump-probe experiments, again using the same femtosecond laser synchronized to the SRS operated in single-bunch mode, were used to probe the carrier dynamics

of the $(10\bar{1}0)$ (m-plane) ZnO surface. These experiments used the frequency-doubled output of the Ti:sapphire oscillator at 360 nm (3.44 eV) to photoexcite the ZnO sample (with a band-gap energy of 3.4 eV).[18] The low-lying Zn $3d$ core level was used to measure the pump-induced change in the SPV.

A shift of the core-level photoelectron spectrum to higher BE of 115 meV was measured with a pump laser fluence of 6.6 nJ cm^{-2}. A shift to higher BE is expected for an n-type oxide with a depletion layer at the surface (Fig. 1). This shift was removed in the absence of laser illumination. As we discuss below, under the conditions of our experiment, we measure the behavior of a nonstoichiometric ZnO_{1-x} surface with a surface oxygen vacancy concentration of 10^{11}–10^{12} cm^{-2}, and our results indicate the presence of a depletion layer, in common with other studies.[3,24] While it has recently been argued that electron accumulation is intrinsic at ZnO surfaces, we anticipate that much lower surface defect concentrations would be required for its observation, as in other TCOs.[3]

In contrast with measurements from silicon, no decay of the SPV was observed over the 320 ns time window of the SRS as shown in Fig. 5(a). This indicates that the charge carrier dynamics occur over much longer timescales in ZnO compared with Si. After photoexcitation, no decay of the SPV shift occurs before the next laser pulse arrives, with the result that a constant SPV shift is measured across the 320 ns time window, including $t = 0$. A power dependence study [Fig. 5(b)] was carried out to verify the relation given by Eq. (5). The SPV depends logarithmically on the laser fluence (and hence the number of induced charge carriers), as is typically observed for smaller gap semiconductors such as silicon.[89]

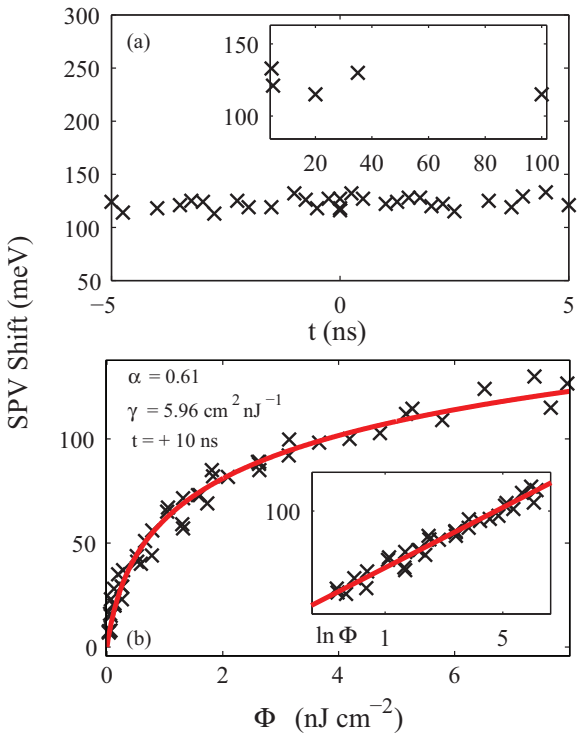

FIG. 5. (Color online) (a) Surface photovoltage shift of the Zn $3d$ core level of the ZnO m-plane surface studied at the SRS, under photoexcitation with 3.44 eV laser pulses with a fluence of 6.6 nJ cm^{-2}. No decay in the pump-induced SPV decay is seen over the time window of the SRS. (b) Power dependence of the pump-induced SPV change at a pump-probe delay time of 10 ns. The inset shows the SPV shift plotted against $\ln\Phi$. The data are fitted using Eq. (5) with $\alpha = 0.61$ and $\gamma = 5.96$ cm^2 nJ^{-1}.

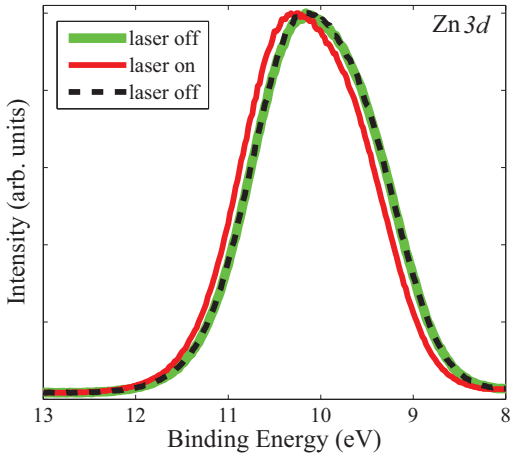

FIG. 6. (Color online) The Zn $3d$ core level of the ZnO m-plane surface recorded using a photon energy of 140 eV with (red line) and without (green and dashed lines) laser photoexcitation with a CW laser (372 nm, 10 mW). The semicore Zn $3d$ level has a complex peak shape influenced by interaction with VB states[90] and is consistent with previous studies of this surface.[91]

These experiments indicate that the SPV decay at the ZnO $(10\bar{1}0)$ surface occurs on timescales in excess of several hundred nanoseconds. In order to understand this phenomenon, we have carried out time-resolved XPS using the experimental arrangement at the TEMPO beamline at Synchrotron-SOLEIL (described in Sec. II A), where SPV changes on timescales from hundreds of nanoseconds to seconds can be measured. Here, a CW laser operating at 372 nm (3.33 eV) was used to photoexcite the sample. The laser was modulated by a signal generator that was also used to trigger the data acquisition software. The laser was typically modulated every 0.5–2 ms, allowing the onset as well as the decay of the SPV shift to be measured. The SPV shift was measured using the peak maximum of the Zn $3d$ signal, and checks were again made to ensure that the shift was exactly removed in the absence of laser illumination (Fig. 6).[90,91] No SPV shift was observed when the experiments were repeated with significantly subband-gap radiation, for example at 590 nm (2.1 eV); subband-gap excitation is discussed further below.

To investigate the remarkably slow decay of the SPV, the effect of a change in sample preparation conditions was explored. As oxygen vacancies have been implicated in the PPC of ZnO,[33–36,40] the influence of a change in the concentration of oxygen vacancies (and hence donors), achieved by altering the length of the oxygen annealing cycle, was investigated. Figure 7 shows the effect of changing the length of this part of the annealing cycle from 20 to 10 min [Figs. 7(a) and 7(b), respectively]. All other experimental conditions are identical. For the 20 min oxygen anneal case, the BE of the Zn $3d$ peak is plotted as the laser is switched on at 0 ms and off after 0.5 ms [shown in the magnified section of Fig. 7(a)]. When the laser is switched on, a total core-level shift

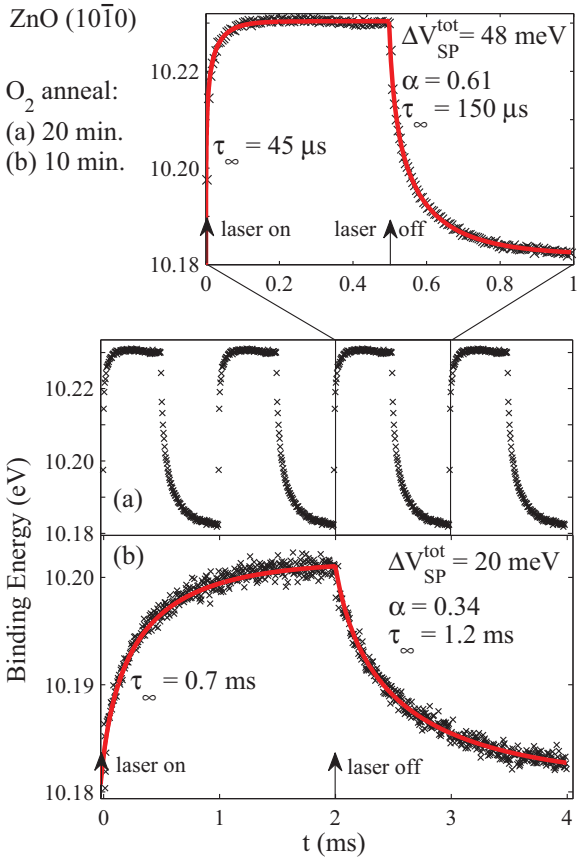

FIG. 7. (Color online) Binding energy shift of the Zn 3*d* core level of the ZnO *m*-plane surface recorded using a photon energy of 140 eV, during modulation of 3.33 eV CW illumination for a minimum of 10 000 data accumulations. Laser modulation is indicated by arrows. The samples were prepared identically (as described in Sec. II B) except for annealing in $1.2–1.4 \times 10^{-7}$ mbar oxygen at 703 K for (a) 20 min and (b) 10 min [the experimental data in (a) are shown repeated on the time axis in the middle panel for comparison with (b)]. The decay and onset of the pump-induced SPV are fitted using Eq. (4) and an analogous decelerating exponential increase, respectively (red lines). Reducing the oxygen annealing time from 20 to 10 min leads to an increase in the dark carrier lifetime τ_∞ of approximately one order of magnitude.

of 48 meV to higher BE is observed, but the rise time of the shift is very long. The SPV shift reaches its maximum value after approximately 0.1 ms. When the laser is switched off, the SPV shift decays back to equilibrium slowly, over almost 0.5 ms.

We use self-decelerating relaxation models to obtain characteristic lifetimes for both the SPV onset and its decay. Equation (4), rather than Eq. (3), was found to provide the best fit of the decay of the pump-induced SPV. This is because, in this experiment, the total SPV shift of 48 meV is comparable to kT (∼26 meV), requiring use of the more general form of the expression for SPV shift [in place of Eq. (3) used for the silicon data]. Likewise, a decelerating exponential increase, analogous to Eq. (4), fitted the onset of the SPV shift well, as discussed in Appendix D. A similar value for the material parameter α (0.61) was obtained as in the experiments conducted on this surface at the SRS [Fig. 5(b)]. A much larger time constant for

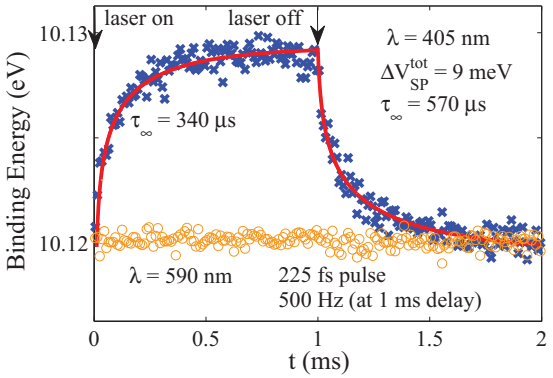

FIG. 8. (Color online) Binding energy shift of the Zn 3*d* core level of the ZnO *m*-plane surface recorded using a photon energy of 140 eV, during modulation of 3.06 eV (405 nm) CW laser illumination (blue crosses) for a minimum of 10 000 data accumulations. The sample was prepared as in Fig. 7(b). Continuous wave laser modulation is indicated by arrows. A dark carrier lifetime τ_∞ of 570 μs is obtained by fitting with the self-deceleration model of Eq. (4). Also shown is the BE of the Zn 3*d* core level during illumination with 590 nm (2.10 eV) radiation (orange circles). Here, a pulsed laser (225 fs pulse width) was modulated at 500 Hz, i.e., every 2 ms, with a delay of 1 ms.

the SPV shift of 1.2 ms [approximately an order of magnitude larger than that shown in Fig. 7(a)] is found when the oxygen annealing time is reduced [Fig. 7(b)].

The change in the oxygen annealing treatment of the substrate changes the timescales of the slow SPV decay by approximately an order of magnitude, with the slowest SPV decay time found in the less oxygenated surface. We also note that this surface shows a smaller SPV shift; an SPV shift of 20 meV is measured in Fig. 7(b) (10 min oxygen anneal), compared with 48 meV in Fig. 7(a) (20 min oxygen anneal). The material parameter α decreases from 0.61 to 0.34 as the oxygen annealing time is halved. The increase in τ_∞ from a few hundred microseconds to around 1 ms on decreasing the oxygen annealing time in this way was found to be reproducible in several different experiments conducted on successive synchrotron beam runs.

In order to explore the possible role of oxygen-vacancy-related band-gap states in PPC,[40] separate experiments were also conducted using subband-gap excitation to excite a sample prepared in a similar way to that in Fig. 7(b), i.e., annealed in oxygen for 10 min. A pulsed laser of significantly subband-gap energy (wavelength 590 nm, or 2.10 eV) was used to illuminate the sample every 2 ms at a delay of 1 ms. No change in the position of the Zn 3*d* peak was observed (Fig. 8); these laser pulses do not have enough energy to photoexcite electrons across the band gap of 3.4 eV or to excite the broad 2.5 eV GD band.[35] However, a small photoresponse with τ_∞ of 570 μs was measured following 405 nm (3.06 eV) excitation (Fig. 8). The observation of PPC using slightly subband-gap radiation is consistent with observations from ZnO nanowires.[40,92,93]

V. DISCUSSION

The change in the surface potential caused by photoexcitation has been observed on two dramatically different

timescales. A Si (111) 7×7 surface was found to show a SPV shift that decayed with a time constant of 6.6 μs, whereas an m-plane ZnO ($10\bar{1}0$) sample showed much slower onset and decay constants spanning hundreds of microseconds or even milliseconds, i.e., three orders of magnitude slower.

For the silicon surface, the data are well fitted by the self-decelerating relaxation model used by Widdra *et al.*,[48] without the need to invoke an additional fast (few nanoseconds) component such as that found by Ogawa *et al.*[52] The equilibrium band bending so calculated is consistent with the known electronic structure of this surface. By removing the background due to preceding pulses from the SPV transient, we obtain a value for the dark carrier lifetime that is consistent with literature values.[52,85,94] We also observe no discontinuities in the decay at subnanosecond timescales that might suggest the presence of fast decay channels mediated by surface states, as is observed for the Si (111) 2×1 surface.[84] Overall, we conclude that, within the timeframe of our experiment, the observed SPV decay for Si (111) 7×7 is explained by recombination of carriers by thermionic emission across the surface depletion layer.

Clearly, very different behavior is observed for ZnO, an n-type TCO. The SPV shift depends logarithmically on laser fluence, as expected for a semiconductor. It may be fitted using the self-decelerating relaxation model, generating a consistent material parameter α. However, very long SPV onset and decay times are measured, and these are clearly strongly affected by the oxygen content of the sample. The magnitude of the SPV decay is also influenced; the SPV becomes larger and the decay faster as the oxygen content increases. The rival explanations for PPC in ZnO (discussed further below) all rely on the availability of oxygen; however, in the oxygen photodesorption model, this is provided from the environment by chemisorption,[24–30] whereas in the models based on metastable band-gap defect states, the concentration of lattice oxygen vacancies controls the PPC.[33–36,40] For nonstoichiometric oxides like ZnO_{1-x}, we know from the phase rule that the lattice oxygen content at a fixed temperature is influenced by the partial pressure of oxygen in the gaseous environment around the sample. This causes difficulty in differentiating these mechanisms in experiments conducted close to ambient pressure. The degree of control afforded by our UHV experiment allows us to distinguish between these proposals, as we describe below.

In the measurements shown in Fig. 7, the residual vacuum during acquisition of the pump-probe data was similar for both ZnO surfaces (around 1.5×10^{-10} mbar). The measurements therefore demonstrate that the SPV dynamics are influenced by the initial number of oxygen vacancies (produced during the preliminary surface preparation) over many thousands of iterations of our experiment. Thus, we begin by estimating these oxygen vacancy concentrations and the corresponding donor concentrations. Unlike other n-type oxides, such as TiO_2, the presence of oxygen vacancies in ZnO does not give rise to a distinct band-gap feature in VB photoemission, and the oxygen vacancy concentration at the surface of vacuum-annealed ZnO ($10\bar{1}0$) has been shown to be very low.[66,72] However, the relationship between the surface oxygen vacancy concentration [V_{OS}] and sample preparation conditions has been established in the seminal and extensive work by Göpel *et al.*[66,67] This allows us to estimate an initial [V_{OS}] after activation of the sample by high-temperature annealing *in vacuo* at 1023 K (at a partial oxygen pressure of 10^{-12} mbar) of 2×10^{12} cm^{-2}, corresponding to a surface site occupancy by vacancies θ of approximately 1.8×10^{-3}.[66] Similarly, the change in surface conductivity with oxygen exposure as a function of time has also been established by Göpel *et al.*[66,95,96] As the conductivity of ZnO varies linearly with donor concentration up to concentrations as high as $\sim 10^{20}$ cm^{-3},[97] we use this work to estimate that the surface oxygen vacancy concentration after 10 min of oxygen annealing in 1.2×10^{-7} mbar O_2 at 703 K is reduced to 0.6×10^{12} cm^{-2}, and after 20 min of annealing is 0.13×10^{12} cm^{-2}.[51,92,93] We assume that the ratio of the corresponding surface donor concentrations is not affected substantially by the subsequent sample treatment and that the defect concentration established in the sample during high-temperature sample preparation is quenched in subsequent room temperature measurements. Using Eq. (1), we may then estimate the change in equilibrium band bending induced by oxygen annealing in our experiment:

$$\ln\left(\frac{\Delta V_{SP}^{tot}(10)}{\Delta V_{SP}^{tot}(20)}\right).\frac{\Delta V_{SP}^{tot}(10)}{\Delta V_{SP}^{tot}(20)} = \ln\left(\frac{n(10)}{n(20)}\right).\frac{V_0(10)}{V_0(20)}, \quad (6)$$

where $\Delta V_{SP}^{tot}(10,20)$, $n(10,20)$, and $V_0(10,20)$ are, respectively, the total pump-induced SPV, donor concentration, and equilibrium band bending at surfaces annealed in oxygen for (10, 20) min. Here, we have assumed that the photoexcited carrier concentration is constant, as constant laser fluence was maintained between experiments. We obtain $V_0(20) \sim 4.2 \times V_0(10)$. This is consistent with the measured change in α (shown in Fig. 7), assuming a similar relationship between these quantities as found for Si.[78] Together with the relationship for the change in equilibrium band bending ΔV_0 with donor concentration:[98]

$$\Delta V_0 = -kT \ln\left[\frac{n(20)}{n(10)}\right], \quad (7)$$

we obtain $V_0(10) \sim 43$ meV and $V_0(20) \sim 180$ meV, both consistent with the experimentally observed $\Delta V_{SP}^{tot}(10,20)$ values of 20 and 48 meV, respectively. Thus, the surface conductivity is higher and the equilibrium band bending lower at the surface with the higher [V_{OS}] as we would expect. Photoexcitation of the surface acts to lower the barrier further, analogous to applying a forward bias to a Schottky diode; complete band-flattening is not achieved in either case. The observation of slower dynamics for the less oxygenated surface is thus all the more remarkable, as if the dynamics were controlled solely by the probability of thermionic emission across the surface depletion layer as for Si, then we would expect the rate of recombination k_r to be given by[98]

$$k_r \propto n_D \exp\left[\frac{-(V_0 - \Delta V_{SP})}{kT}\right], \quad (8)$$

i.e., proportional to the concentration of donors n_D and the probability of an electron crossing the surface barrier to recombine with a hole. These are both factors that are larger for the surface with higher [V_{OS}].

Clearly, some process other than thermionic emission controls the observed dynamics in ZnO. Because of the importance of ZnO as a gas sensor material, its photoconductivity has been studied extensively.[9,25–31,92] Persistent photoconductivity has been observed frequently; photoconductive changes over minutes and even hours are often reported.[9,24,27–31,92] In our experiments, the observed BE provides a measure of the surface conductivity [because the high surface conductivity associated with low band bending corresponds to high BE in Fig. 7,[9] while surfaces showing high band bending (low BE in our experiments) have low conductivity]. Indeed, the SPV transients of Fig. 7 show a striking resemblance to the photoconductivity transients recorded by Bao *et al.*[31] and Keem *et al.*[92] for UV-illuminated ZnO nanowires and by Hou *et al.*[9] for ZnO nanowires where charge is injected into the ZnO CB by charge injection from photoexcited CdSe quantum dots.

This behavior in ZnO has for some time been attributed to the chemisorption and photodesorption of oxygen at the surface;[24–30] alternative mechanisms involving metastable band-gap defect states associated with oxygen vacancies have been proposed more recently,[33–36,40] and some experimental evidence supporting the involvement of these defect states has emerged.[36,40,93] In the oxygen photodesorption model, oxygen molecules chemisorb onto the ZnO surface primarily at undercoordinated surface Zn sites.[31,99,100] The molecules become negatively charged ions (O_2^-) by capturing donor electrons from the *n*-type ZnO substrate, creating a depletion layer at the surface that causes band bending. Upon photoexcitation, electron-hole pairs are created when electrons are promoted into the CB. The holes migrate to the surface (under the influence of the surface potential) and discharge oxygen ions causing desorption of molecular oxygen from the surface [$h^+ + O_2^- \rightarrow O_2(g)$, where ($g$) denotes the gas phase].[26] The electrons migrate in the reverse direction, into the bulk, enhancing the photoconductivity, and the band bending is reduced. After photoexcitation, the rate of recombination is limited by the absence of holes caused by the oxygen desorption process.[26] The equilibrium band bending is restored by oxygen chemisorption at the surface involving the capture of carriers across the depletion layer.[24,26,30] This cycle is illustrated in Fig. 9.

In this model, the timescale of the SPV decay is limited by the rate of adsorption of O_2 from the gas phase, reestablishing a chemisorbed layer of O_2^- (with its associated depletion layer) at the ZnO surface:[100]

$$Zn_{Zn,s} + O_2(g) + e^-(Zn_{Zn}O_2^-)_s \qquad (9)$$

$Zn_{Zn,s}$ is an undercoordinated zinc atom in the surface layer that may act as an adsorption site and $(Zn_{Zn}O_2^-)_s$ is the adsorption complex. The controlled UHV environment of our experiment, where we can estimate the rate of arrival of O_2 molecules at the ZnO surface, allows us to test this model. If we assume that O_2 adsorbs only at the vacancy sites with unity sticking probability,[72] then in a partial pressure of O_2 of 10^{-12} mbar, timescales of the order of 100 s are required to fill all the vacancies at the surface shown in Fig. 7(a) (annealed for 20 min in O_2), and a correspondingly longer time for the more defected surface in Fig. 7(b). Other molecules, such as hydrocarbons (forming CO_2) have been implicated in the chemisorptions-photodesorption mechanism.[31,101] However,

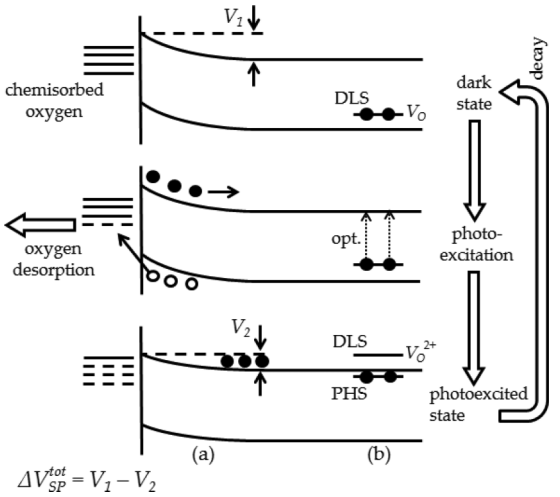

FIG. 9. Schematic diagram of the processes occurring following photoexcitation of ZnO. The pump-induced SPV measured is the difference in the amount of band bending between the dark and photoexcited states $\Delta V_{SP}^{tot} = V_1 - V_2$. Filled circles denote electrons and open circles denote holes. (a) Oxygen photodesorption mechanism for PPC: the oxygen-related surface states are shown by solid and dashed lines denoting filled and empty states, respectively.[24] (b) Persistent photoconductivity mediated by band-gap states associated with metastable doubly charged oxygen vacancies: the process of carrier photoexcitation from a DLS is shown by the vertical arrows; this releases two electrons to the shallow PHS.[32]

even if we assume that every species in the residual vacuum of the UHV chamber can chemisorb at the surface and abstract holes, there remains a disparity of a factor of 10^3–10^4 between the observed timescales of PPC (Fig. 7) and those predicted by the photodesorption mechanism. Thus, our measurements clearly demonstrate that, under the conditions of our experiment, the oxygen photodesorption mechanism is not the dominant mechanism of PPC.

The measurement of PPC using subband-gap excitation here (Fig. 8) and in measurements from ZnO nanowires[36,40,93] and the dependence we observe on the initially introduced [V_O] are difficult to reconcile with the oxygen photodesorption mechanism. Both lend support to alternative mechanisms for PPC involving band-gap states associated with metastable doubly[21,32,33] or singly charged[34] oxygen vacancy states. A consensus of opinion is emerging that the un-ionized oxygen vacancy state V_O is a defect-localized state (DLS) lying deep in the band gap[3,20] and is a very efficient hole trap.[33] However, modeling studies[32] show that metastable ionized oxygen vacancy states should have energies close enough to the CB minimum (CBM) to contribute to conductivity. This has led to the emergence of an alternative model for PPC. Lany and Zunger[32] suggest that the energy of the doubly ionized vacancy V_O^{2+} lies above the CBM; on photoexcitation, the electrons in the occupied DLS are promoted to occupy a metastable perturbed host state (PHS) resonant with the CBM (created by the BE between the photoexcited electrons in the CB and the V_O^{2+} state, Fig. 9). This leads to a configuration change (primarily a shortening of the Zn-Zn bond distances), such that there is an activation energy barrier of approximately 0.2 eV to return to the ground state; two electrons must also

be captured by the V_O^{2+} state.[32] The difficulty of meeting these conditions simultaneously leads to PPC.[102]

As in the oxygen photodesorption mechanism, the rate of decay of PPC depends on the rate of recombination of the photoexcited electrons with holes, and thus inversely on the concentration of hole traps. Now, the main hole traps are the unionized V_O (rather than surface O_2^-),[103] thus the PPC persists for longer times as the oxygen vacancy concentration increases, as we observe. We note that a number of studies have shown that oxygen vacancies are more stable at or near the surface than in the bulk;[31,35,104] given the field gradient at the surface (Fig. 9), this suggests that most of the hole trapping occurs close to the surface. We observe no change in the measured SPV shifts over the tens of thousands of photoexcitation cycles necessary in our experiment (Fig. 7), or after repeated measurements. This is consistent with a mechanism dependent on the initially introduced $[V_O]$, but inconsistent with the oxygen photodesorption mechanism (as we would expect the surface to become depleted of chemisorbed oxygen in UHV after very few photoexcitation cycles). We note that the dynamics observed in ambient pressure experiments are also strongly dependent on the availability of oxygen, being significantly slowed (to many hours) in vacuum or an inert gas.[9,31] This has been used to support the oxygen photodesorption mechanism, but as we noted above, for a nonstoichiometric oxide, $[V_O]$ is also influenced by the partial pressure of oxygen surrounding the sample; our experiments allow these effects to be deconvoluted.

The oxygen photodesorption model implies that photoconductivity in ZnO requires photons with energies at least as large as the band gap. As band-gap states are implicated in the oxygen vacancy mechanism, PPC mediated via this mechanism should be observable using subband-gap radiation, as observed here (Fig. 8) and in measurements from ZnO nanowires.[36,40,93] Our observation of PPC using 405 nm radiation (3.06 eV, cf. the ZnO band gap of 3.4 eV) is consistent with the conductance onset observed at 410 nm (3.02 eV) by Liu *et al.*[40] (and attributed by these authors to V_O states lying at around 240 meV above the VB edge). Our experiments reveal similar slow dynamics for subband-gap (405 nm) and band-gap excitation, showing that these oxygen-vacancy-related band-gap states are directly associated with the PPC.[105] Taking a value for the bulk band gap of 3.4 eV,[3,7,18] these defect states lie approximately 340 meV above the VB edge, consistent with the range of energies identified by Liu *et al.*[40] The true nature of these states has still to be determined; for example, the involvement of hydrogen at V_O sites[37] cannot be excluded.

Our results show that carrier recombination at the *m*-plane ZnO surface is orders of magnitude slower than in conventional semiconductors such as silicon. The resulting timescales (in the microsecond to millisecond range) are akin to those normally associated with carrier transport. These results have important consequences for the fabrication of next-generation solar cells using ZnO, for example as photoanode. These devices rely on charge injection from a photosensitizer (such as a dye or quantum dot) into the photoanode.[9] Current indications are that charge injection into oxide photoanodes is fast (occurring on femtosecond timescales).[106] Our results show that, once injected into the CB of ZnO, the lifetime of the photoexcited carrier may be very long, making it competitive with the times taken for transport through the photoanode to the back contact. This means that ZnO photoanodes are highly suitable for efficient transport of photocurrent, contributing to the external quantum efficiency of the device.

VI. CONCLUSIONS

We have compared the photoexcited carrier dynamics in the archetypal photovoltaic Si [using the Si (111) 7×7 surface], with those at the surface of a potential next-generation photoanode material, ZnO [using the nonpolar *m*-plane $(10\bar{1}0)$ surface]. Two laser-pump x-ray-probe experiments have been used, one measuring changes over a 320 ns time window with subnanosecond resolution, and one over much longer millisecond timescales, with a resolution of 150 ns. The two photovoltaics studied have formally similar electronic structures, but nevertheless show very different charge carrier dynamics. The pump-induced SPV at the Si (111) 7×7 surface is found to decay with a time constant of 6.6 μs and is well modeled by the self-decelerating relaxation model.[48,49] Our analysis demonstrates the importance of removing the background due to preceding pulses from the SPV transient. We find no evidence of a shorter (nanosecond or subnanosecond) component, and conclude that, over the timescales of our experiment, the decay is explained by recombination of carriers by thermionic emission across the surface depletion layer. The SPV shift at the ZnO $(10\bar{1}0)$ surface is logarithmically dependent on laser fluence, as is typically observed for smaller gap semiconductors. The SPV decay may again be fitted by a self-decelerating model, but the SPV decay time is much longer (typically hundreds of microseconds), i.e., PPC is observed. However, calculation of the oxygen arrival rate at the surface in our UHV chamber allows us to demonstrate that, under the conditions of our experiment, the oxygen photodesorption mechanism is not the dominant mechanism of PPC. The decay time of the PPC is sensitively dependent on oxygen vacancy concentration, and may be changed by approximately an order of magnitude by changes in the conditions used to prepare the surface. The magnitude of the SPV decay is also influenced; the SPV becomes larger and the PPC decay faster as the surface is oxygenated. Persistent photoconductivity is also observed when the surface is illuminated with subband-gap (405 nm) radiation, revealing that defect states approximately 340 meV above the VB edge are directly associated with the PPC. These observations support the hypothesis that ionized oxygen vacancy states are responsible for the PPC.[32] The results suggest that ZnO is highly suited as a photoanode material in next-generation solar devices.

Laser-pump x-ray-probe measurements are powerful probes of photoexcited carrier dynamics over a wide range of timescales; indeed, the contrasting dynamics exhibited by the two photovoltaics probed here indicate a need for further studies in this area.

ACKNOWLEDGMENTS

Work carried out at the SRS was supported by the Science and Technologies Facilities Council, UK, and the North West

Science Fund of the UK's North West Development Agency. Work was also supported by the Cockcroft Institute via its STFC core grant ST/G008248/1. The research leading to these results has also received funding from the European Community's Seventh Framework Programme (FP7/2007-2013) under grant agreement no. 226716, allowing access to Synchrotron-SOLEIL.

APPENDIX A: MEASUREMENTS FROM *p*-TYPE Si (111) 7 × 7 SURFACES

A boron-doped *p*-type silicon sample (resistivity 4 Ω cm) was used to observe the SPV change upon photoexcitation in a conventional *p*-type semiconductor. Figure 10 shows that the Si 2*p* core level is shifted to lower BE (higher KE) upon photoexcitation. This is in contrast to measurements on the *n*-type surface (Fig. 2) where core level binding energies are increased. This is consistent with the presence of an accumulation layer (and downward band bending) at the *p*-type Si (111) 7 × 7 surface, and contrasts with the observation of a depletion layer (and upward band bending) at the *n*-type Si (111) 7 × 7 surface.

APPENDIX B: Si (111) TRANSIENT SPV FITTING

The transient SPV is fitted according to the simplified constant deceleration model ($\Delta V_{SP}^{tot} \gg kT$) from Bröcker:[49]

$$\Delta V_{SP}(t) = -\alpha kT \ln\left[\exp\left(\frac{-\Delta V_{SP}^{tot}}{\alpha kT}\right) + \frac{t}{\tau_\infty}\right]. \quad \text{(B1)}$$

However, the SPV transient lies on a time-varying background of approximately 345–300 meV because the equilibrium band bending is not reached within the 320 ns time

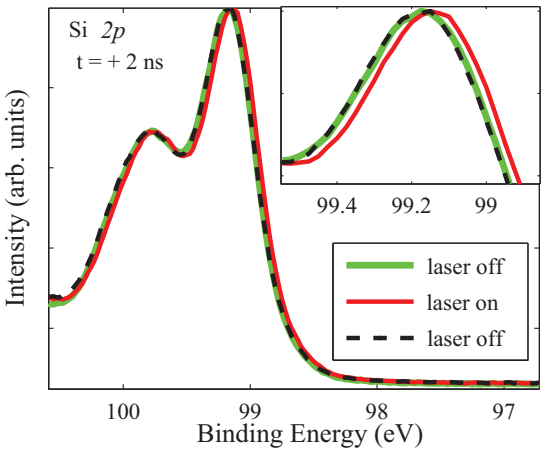

FIG. 10. (Color online) The Si 2*p* core level spectrum of a *p*-type Si (111) 7 × 7 surface, obtained using a photon energy of 140 eV. The Si 2*p* core level shifts to lower BE ($\Delta V_{SP} = 40$ meV) upon photoexcitation with 402 nm laser pulses (at a fluence of 9.53 nJ cm^{-1} and a pump-probe delay time of 2 ns before the x-ray probe). This is consistent with an accumulation layer at the semiconductor surface. Spectra without laser photoexcitation taken before (green line) and after (black dashed line) the laser-on spectrum show that the peak returns to its original BE after photoexcitation (the spectra overlie each other).

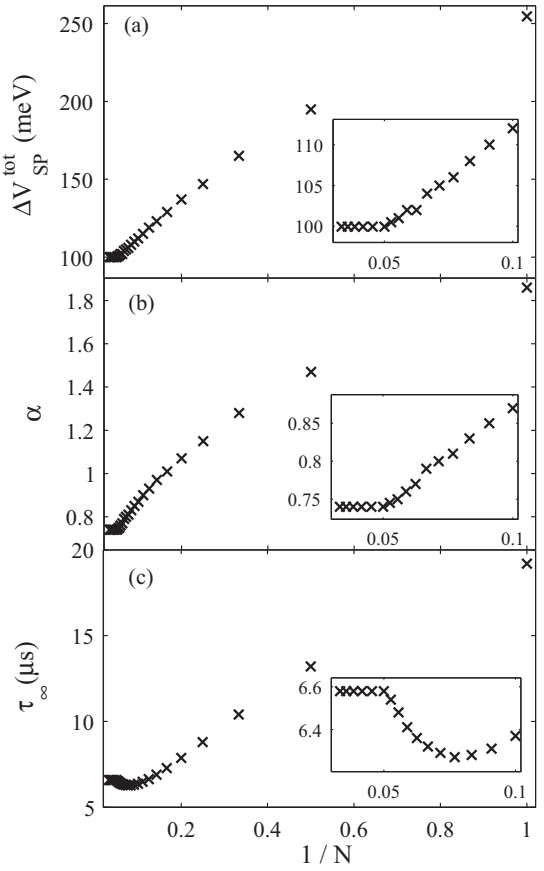

FIG. 11. Convergence of (a) the total SPV shift ΔV_{SP}^{tot}, (b) the material parameter α, and (c) the dark carrier lifetime τ_∞ for increasing numbers of previous pulses included in the model ($N = 1$ to 30). The parameters converge at 100 meV, 0.74, and 6.6 μs, respectively.

window of the SRS. Therefore, to fit the data according to Eq. (B1), removal of the background due to preceding pump pulses is required. The model is adapted as follows:

$$\Delta V_{SP}(t) = \Delta V_{SP}(t) + \sum_{n=1}^{N} \Delta V_{SP}(t + nT), \quad \text{(B2)}$$

where T is the time period, here 320 ns; N is the number of previous photoexcitations included in the model, which must be large enough such that all the previous pulses that affect the current decay are included. Increasing N allows for a convergence study to be carried out. Figure 11(a) shows how the total SPV shift ΔV_{SP}^{tot}, (b) the material parameter α, and (c) the dark carrier lifetime τ_∞ vary as N is increased. Convergence is reached at $N = 20$ ($1/N = 0.05$) i.e., including more previous photoexcitations does not change the fitting, because these laser pulses are not affecting the current photoexcitation decay. This is consistent with the fitted dark carrier lifetime of 6.6 μs (<320 ns × 21 pulses).

The background due to preceding pump pulses has a significant influence on the transient SPV, shown in Fig. 12 where the model for the preceding 20 pulses [Eq. (B2)] has been subtracted from the raw transient SPV data. The effect of the preceding pulses on the onset of the SPV is shown in Fig. 12(b), where the observed SPV maximum is reduced and

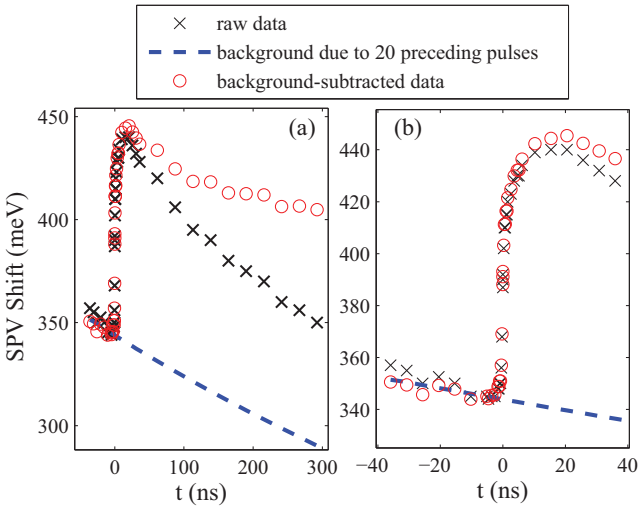

FIG. 12. (Color online) (a) The pump-induced change in the SPV for an n-type Si (111) 7×7 surface, excited with 800 nm radiation and (b) the SPV onset before (black crosses) and after (red circles) the subtraction of the background due to 20 preceding laser pump pulses (blue dotted line). The corrected data are shown added to a constant offset of 345 meV (corresponding to the background height at $t = 0$) for ease of comparison.

broadened by the effect of the preceding pulses. This reduces the confidence in any conclusions drawn about the behavior of the surface at short (<20 ns) delay times. At longer delay times, there is a significant divergence between the corrected data and the raw data [Fig. 12(a)], and it is clear that fitting the raw data with Eq. (B1) would lead to a considerably underestimated lifetime. This illustrates the importance of correction of the raw SPV data for the influence of preceding pump pulses.

APPENDIX C: CALCULATION OF THE POSITION OF THE VB MAXIMUM AT THE Si (111) 7 x 7 SURFACE

To determine whether the value of the maximum laser-induced SPV obtained from the fitting procedure (shown in Fig. 4) is consistent with the magnitude of the equilibrium band bending at the surface requires knowledge of the position of the Fermi level within the bulk of the material and the pinning position at the surface. Within the bulk of the material, the position of the Fermi level E_F below the CBM (E_C) is given by:[98]

$$E_C - E_F = kT \ln\left(\frac{n_C}{n_D}\right), \tag{C1}$$

where n_D is the dopant concentration and n_C is the density of states function multiplied by the Fermi-Dirac distribution function and integrated from the CB edge to infinity (commonly referred to as the CB effective density of states).[98] The latter is 2.8×10^{19} cm^{-3} for n-type, phosphorus-doped silicon.[98] The former can be obtained from the resistivity of the sample ($5 \pm 2\ \Omega$ cm), which corresponds to a doping level of 1×10^{15} cm^{-3} for n-type silicon.[107] Here, $(E_C - E_F)$ is thus determined to be 0.26 eV at 300 K. The equilibrium band banding V_0 obtained using Eq. (1), for a SPV of 100 meV, is

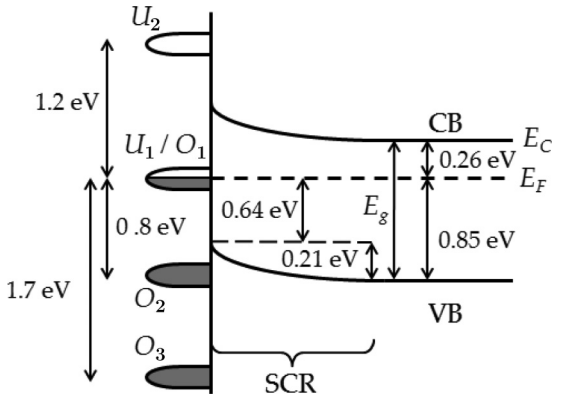

FIG. 13. Schematic diagram of the electronic structure at the Si (111) 7×7 surface. There are partially filled surface states at the Fermi level (U_1/O_1), with a second unoccupied surface state 1.2 eV above the Fermi level, as well as two occupied states 0.8 and 1.7 eV below the Fermi level.[15,108,109] The equilibrium band bending V_0 across the space charge region (SCR) is determined to be 0.21 eV.

0.21 eV. Therefore, the Fermi level is 0.64 eV above the VB maximum at the surface, as shown in Fig. 13.

In Fig. 13, we also show schematically the energies of the occupied and unoccupied surface states at the Si (111) 7×7 surface, using values and assignments from the literature.[15,108,109] The partially filled states at the Fermi energy (unoccupied labeled U_1 and occupied O_1) arise from the surface adatom dangling bonds, which give rise to the S_2 component of the Si $2p$ spectrum shown in Fig. 3.[108,110,111] The occupied state marked O_2 at approximately 0.8 eV below E_F is due to the dangling bonds of the rest atoms; these atoms give rise to the S_5 component in the Si $2p$ spectrum.[108,110,111] The O_3 state at approximately 1.7 eV below E_F is due to adatom backbonding to the bulk and also has a small contribution from surface dimers; this is linked with the S_3 and S_4 components of the Si $2p$ spectrum. The adatom antibonding component lies 1.2 eV above E_F (marked U_2).

APPENDIX D: ZnO (10$\bar{1}$0) TRANSIENT SPV FITTING

We use the self-decelerating relaxation model to obtain characteristic lifetimes for the SPV decay, as for the Si (111) 7×7 surface. Equation (4) is found to be necessary to fit these data, as described in Subsec. IV.B. This validates the proposal by Bröcker *et al.*[49] for the functional form of $\Delta V_{SP}(t)$ when $\Delta V_{SP}^{tot} \sim kT$. Treatment of the initial onset of the SPV when the laser is switched on is complicated by the constant rate of photogeneration of carriers produced by the CW laser illumination, which competes with recombination processes. As a result, the measured time constants are expected to be shorter than for the SPV decay, as we observe (Figs. 7 and 8). If the optical generation term dominates (for example, if high-intensity illumination is used), then the onset of the SPV transient may be fitted using a simple exponential that yields a time constant inversely proportional to the intensity of illumination.[42] The onset data shown in Figs. 7 and 8 may not be fitted in this way, indicating that the laser fluence is not sufficiently high for the optical generation to completely dominate the charge dynamics. In contrast to the SPV decay

data, it is possible to fit the SPV onsets using a bi-exponential fit, yielding two time constants. However, as the physical significance of these time constants is unclear, we have chosen instead to fit the SPV onset data to a decelerated exponential model analogous to Eq. (4). This reflects the dynamic increase in recombination rate as the surface band bending is reduced, which acts to counterbalance the rate of carrier photogeneration (i.e., the slowing of the dynamics after the laser is switched on is an intrinsic part of the physics of the junction). This yields the values for τ_∞ (the characteristic timescale associated with photogeneration) shown in Figs. 7 and 8.

*Corresponding author: ben.spencer@manchester.ac.uk
†Present address: Manchester Institute of Biotechnology, Faculty of Life Sciences, University of Manchester, 131 Princess Street, Manchester M1 7DN, United Kingdom.
‡Present address: School of Chemistry, The University of Nottingham, University Park, Nottingham, NG7 2RD, United Kingdom.
§Present address: Nanoco Technologies Ltd., Grafton Street, Manchester M13 9NT, United Kingdom.
‖Present address: Sri Lanka Institute of Nanotechnology (SLINTEC), Nanotechnology and Science Park Mahenwatte, Pitipana, Homagama, Colombo, Sri Lanka.

[1]M. A. Green, J. H. Zhao, A. H. Wang, and S. R. Wenham, IEEE Trans. Electron Devices **46**, 1940 (1999).
[2]T. Saga, Npg Asia Mater **2**, 96 (2010).
[3]P. D. C. King and T. D. Veal, J. Phys.: Condens. Matter **23**, 334214 (2011).
[4]C. Wadia, A. P. Alivisatos, and D. M. Kammen, Environ. Sci. Technol. **43**, 2072 (2009).
[5]J. F. Wager, Science **300**, 1245 (2003).
[6]A. P. Ramirez, Science **315**, 1377 (2007).
[7]C. F. Klingshirn, *Zinc Oxide: From Fundamental Properties Towards Novel Applications*. (Springer, Heidelberg, London, 2010).
[8]J. Heber, Nature **459**, 28 (2009).
[9]D. C. Hou, A. Dev, K. Frank, A. Rosenauer, and T. Voss, J. Phys. Chem. C **116**, 19604 (2012).
[10]B. Carlson, K. Leschkies, E. S. Aydil, and X. Y. Zhu, J. Phys. Chem. C **112**, 8419 (2008).
[11]S. J. O. Hardman, D. M. Graham, S. K. Stubbs, B. F. Spencer, E. A. Seddon, H. T. Fung, S. Gardonio, F. Sirotti, M. G. Silly, J. Akhtar, P. O'Brien, D. J. Binks, and W. R. Flavell, Phys. Chem. Chem. Phys. **13**, 20275 (2011).
[12]J. Akhtar, M. A. Malik, P. O'Brien, K. G. U. Wijayantha, R. Dharmadasa, S. J. O. Hardman, D. M. Graham, B. F. Spencer, S. K. Stubbs, W. R. Flavell, D. J. Binks, F. Sirotti, M. El Kazzi, and M. Silly, J. Mater. Chem. **20**, 2336 (2010).
[13]C. Klingshirn, J. Fallert, H. Zhou, J. Sartor, C. Thiele, F. Maier-Flaig, D. Schneider, and H. Kalt, Phys. Status Solidi B **247**, 1424 (2010).
[14]J. P. Long and V. M. Bermudez, Phys. Rev. B **66**, 121308 (2002).
[15]M. Mauerer, I. L. Shumay, W. Berthold, and U. Hofer, Phys. Rev. B **73**, 245305 (2006).
[16]G. Le Lay, M. Gothelid, T. M. Grehk, M. Bjorkquist, U. O. Karlsson, and V. Y. Aristov, Phys. Rev. B **50**, 14277 (1994).
[17]G. Le Lay, A. Cricenti, C. Ottaviani, C. Hakansson, P. Perfetti, and K. C. Prince, J. Electron Spectrosc. Rel. Phen. **88**, 711 (1998).
[18]J. A. McLeod, R. G. Wilks, N. A. Skorikov, L. D. Finkelstein, M. Abu-Samak, E. Z. Kurmaev, and A. Moewes, Phys. Rev. B **81**, 245123 (2010).
[19]J. W. Precker and M. A. da Silva, Am. J. Phys. **70**, 1150 (2002).
[20]A. Janotti and C. G. Van de Walle, Rep. Prog. Phys. **72**, 126501 (2009).
[21]S. Lany and A. Zunger, Phys. Rev. Lett. **98**, 045501 (2007).
[22]C. G. Van de Walle and J. Neugebauer, Nature **423**, 626 (2003).
[23]A. Janotti and C. G. Van de Walle, Nat. Mater. **6**, 44 (2007).
[24]I. Tashiro, T. Kimura, and K. Endo, Appl. Opt. **8**, 180 (1969).
[25]J. Lagowski, E. S. Sproles, and H. C. Gatos, J. Appl. Phys. **48**, 3566 (1977).
[26]A. Rothschild, Y. Komem, and N. Ashkenasy, J. Appl. Phys. **92**, 7090 (2002).
[27]X. G. Zheng, Q. Sh. Li, W. Hu, D. Chen, N. Zhang, M. J. Shi, J. J. Wang, and L. Ch. Zhang, J. Lumin. **122**, 198 (2007).
[28]T. E. Murphy, K. Moazzami, and J. D. Phillips, J. Electron. Mater. **35**, 543 (2006).
[29]R. J. Collins and D. G. Thomas, Phys. Rev. **112**, 388 (1958).
[30]M. J. Liu and H. K. Kim, Appl. Phys. Lett. **84**, 173 (2004).
[31]J. M. Bao, I. Shalish, Z. H. Su, R. Gurwitz, F. Capasso, X. W. Wang, and Z. F. Ren, Nanoscale Res. Lett. **6**, 404 (2011).
[32]S. Lany and A. Zunger, Phys. Rev. B **72**, 035215 (2005).
[33]S. B. Zhang, S. H. Wei, and A. Zunger, Phys. Rev. B **63**, 075205 (2001).
[34]A. Janotti and C. G. Van de Walle, Appl. Phys. Lett. **87**, 122102 (2005).
[35]H. L. Mosbacker, Y. M. Strzhemechny, B. D. White, P. E. Smith, D. C. Look, D. C. Reynolds, C. W. Litton, and L. J. Brillson, Appl. Phys. Lett. **87**, 012102 (2005).
[36]A. Kushwaha and M. Aslam, J. Appl. Phys. **112**, 054316 (2012).
[37]M. H. Du and K. Biswas, Phys. Rev. Lett. **106**, 115502 (2011).
[38]P. D. C. King, T. D. Veal, D. J. Payne, A. Bourlange, R. G. Egdell, and C. F. McConville, Phys. Rev. Lett. **101**, 116808 (2008).
[39]T. Nagata, O. Bierwagen, M. E. White, M. Y. Tsai, and J. S. Speck, J. Appl. Phys. **107**, 033707 (2010).
[40]P. Liu, G. W. She, Z. L. Liao, Y. Wang, Z. Z. Wang, W. S. Shi, X. H. Zhang, S. T. Lee, and D. M. Chen, Appl. Phys. Lett. **94**, 063120 (2009).
[41]M. H. Hecht, Phys. Rev. B **43**, 12102 (1991).
[42]L. Kronik and Y. Shapira, Surf. Sci. Rep. **37**, 1 (1999).
[43]J. E. Demuth, W. J. Thompson, N. J. Dinardo, and R. Imbihl, Phys. Rev. Lett. **56**, 1408 (1986).
[44]J. P. Long, H. R. Sadeghi, J. C. Rife, and M. N. Kabler, Phys. Rev. Lett. **64**, 1158 (1990).
[45]S. Tanaka, S. D. More, J. Murakami, M. Itoh, Y. Fujii, and M. Kamada, Phys. Rev. B **64**, 155308 (2001).
[46]S. Tanaka, T. Nishitani, T. Nakanishi, S. D. More, J. Azuma, K. Takahashi, O. Watanabe, and M. Kamada, J. Appl. Phys. **95**, 551 (2004).
[47]S. Tanaka, T. Ichibayashi, and K. Tanimura, Phys. Rev. B **79**, 155313 (2009).

[48]W. Widdra, D. Bröcker, T. Gießel, I. V. Hertel, W. Kruger, A. Liero, F. Noack, V. Petrov, D. Pop, P. M. Schmidt, R. Weber, I. Will, and B. Winter, Surf. Sci. **543**, 87 (2003).
[49]D. Bröcker, T. Gießel, and W. Widdra, Chem. Phys. **299**, 247 (2004).
[50]T. E. Glover, G. D. Ackermann, A. Belkacem, B. Feinberg, P. A. Heimann, Z. Hussain, H. A. Padmore, C. Ray, R. W. Schoenlein, and W. F. Steele, Nucl. Instrum. Meth. A **467**, 1438 (2001).
[51]T. E. Glover, G. D. Ackermann, Z. Hussain, and H. A. Padmore, J. Mod. Opt. **51**, 2805 (2004).
[52]M. Ogawa, S. Yamamoto, Y. Kousa, F. Nakamura, R. Yukawa, A. Fukushima, A. Harasawa, H. Kondoh, Y. Tanaka, A. Kakizaki, and I. Matsuda, Rev. Sci. Instrum. **83**, 023109 (2012).
[53]A. Vollmer, R. Ovsyannikov, M. Gorgoi, S. Krause, M. Oehzelt, A. Lindblad, N. Martensson, S. Svensson, P. Karlsson, M. Lundvuist, T. Schmeiler, J. Pflaum, and N. Koch, J. Electron Spectrosc. **185**, 55 (2012).
[54]M. Hajlaoui, E. Papalazarou, J. Mauchain, G. Lantz, N. Moisan, D. Boschetto, Z. Jiang, I. Miotkowski, Y. P. Chen, A. Taleb-Ibrahimi, L. Perfetti, and M. Marsi, Nano Lett. **12**, 3532 (2012).
[55]M. Marsi, R. Belkhou, C. Grupp, G. Panaccione, A. Taleb-Ibrahimi, L. Nahon, D. Garzella, D. Nutarelli, E. Renault, R. Roux, M. E. Couprie, and M. Billardon, Phys. Rev. B **61**, R5070 (2000).
[56]M. Marsi, M. E. Couprie, L. Nahon, D. Garzella, T. Hara, R. Bakker, M. Billardon, A. Delboulbe, G. Indlekofer, and A. TalebIbrahimi, Appl. Phys. Lett. **70**, 895 (1997).
[57]S. Yamamoto and I. Matsuda, J. Phys. Soc. Jpn. **82**, 021003 (2013).
[58]D. J. Holder, P. D. Quinn and N. G. Wyles, in *European Particle Accelerator Conference* (JACoW, Genoa, Italy, 2008), p. 2133.
[59]G. C. Idzorek and R. J. Bartlett, in *EUV, X-Ray, and Gamma-Ray Instrumentation for Astronomy VIII* (SPIE, Bellingham, WA, 1997), Vol. 3114, p. 349.
[60]F. Polack, M. Silly, C. Chauvet, B. Lagarde, N. Bergeard, M. Izquierdo, O. Chubar, D. Krizmancic, M. Ribbens, J. P. Duval, C. Basset, S. Kubsky, and F. Sirotti, AIP Conf. Proc. **1234**, 185 (2010).
[61]N. Bergeard, M. G. Silly, D. Krizmancic, C. Chauvet, M. Guzzo, J. P. Ricaud, M. Izquierdo, L. Stebel, P. Pittana, R. Sergo, G. Cautero, G. Dufour, F. Rochet, and F. Sirotti, J. Synchrotron Radiat. **18**, 245 (2011).
[62]G. Cautero, R. Sergo, L. Stebel, P. Lacovig, P. Pittana, M. Predonzani, and S. Carrato, Nucl. Instrum. Meth. A **595**, 447 (2008).
[63]C. Y. Su, P. R. Skeath, I. Lindau, and W. E. Spicer, Surf. Sci. **107**, L355 (1981).
[64]K. Takayanagi, Y. Tanishiro, M. Takahashi, and S. Takahashi, J. Vac. Sci. Technol. A **3**, 1502 (1985).
[65]K. Ozawa and K. Edamoto, Surf. Sci. **524**, 78 (2003).
[66]W. Göpel and U. Lampe, Phys. Rev. B **22**, 6447 (1980).
[67]W. Göpel, Surf. Sci. **62**, 165 (1977).
[68]O. Dulub, L. A. Boatner, and U. Diebold, Surf. Sci. **519**, 201 (2002).
[69]U. Diebold, L. V. Koplitz, and O. Dulub, Appl. Surf. Sci. **237**, 336 (2004).
[70]S. J. Pearton, D. P. Norton, K. Ip, Y. W. Heo, and T. Steiner, Prog. Mater. Sci. **50**, 293 (2005).
[71]J. M. Lee, K. K. Kim, S. J. Park, and W. K. Choi, Appl. Phys. Lett. **78**, 3842 (2001).
[72]V. E. Henrich and P. A. Cox, *The Surface Science of Metal Oxides*. (Cambridge University Press, Cambridge; New York, 1994).
[73]We note that both volume and grain boundary oxygen diffusion in ZnO are facile (Refs. 74 and 75); we expect this change in preparation conditions to be sufficient to influence the oxygen content over the probing depths appropriate to our experiment (a few nanometers). The penetration depth of the laser pump radiation is around 40 nm in ZnO (Ref. 76).
[74]G. W. Tomlins, J. L. Routbort, and T. O. Mason, J. Am. Ceram. Soc. **81**, 869 (1998).
[75]A. C. S. Sabioni, A. M. J. M. Daniel, W. B. Ferraz, R. W. D. Pais, A.-M. Huntz, and F. Jomard, Mater. Res.-Ibero-Am. J. **11**, 221 (2008).
[76]I. S. Jeong, J. H. Kim, and S. Im, Appl. Phys. Lett. **83**, 2946 (2003).
[77]W. A. Tisdale, M. Muntwiler, D. J. Norris, E. S. Aydil, and X. Y. Zhu, J. Phys. Chem. C **112**, 14682 (2008).
[78]J. Schulz, P. Wurfel, and W. Ruppel, Phys. Status Solidi B **164**, 425 (1991).
[79]R. Hesse, P. Streubel, and R. Szargan, Surf. Interface Anal. **39**, 381 (2007).
[80]C. S. Ltd. (www.casaxps.com, 2009).
[81]P. Morgen, U. Hofer, W. Wurth, and E. Umbach, Phys. Rev. B **39**, 3720 (1989).
[82]G. Hollinger and F. J. Himpsel, Appl. Phys. Lett. **44**, 93 (1984).
[83]Fits can also be obtained which show changes in the relative spectral contributions on photoexcitation, but as in no case do these match population changes that could be achieved with relatively low fluence 800 nm illumination, we reject these as unphysical.
[84]M. Marsi, L. Nahon, M. E. Couprie, D. Garzella, T. Hara, R. Bakker, M. Billardon, A. Delboulbe, G. Indlekofer, and A. Taleb-Ibrahimi, J. Electron Spectrosc. **94**, 149 (1998).
[85]R. J. Hamers and D. G. Cahill, Appl. Phys. Lett. **57**, 2031 (1990).
[86]D. L. Meier, J. M. Hwang, and R. B. Campbell, IEEE Trans. Electron Devices **35**, 70 (1988).
[87]F. J. Himpsel, G. Hollinger, and R. A. Pollak, Phys. Rev. B **28**, 7014 (1983).
[88]R. Losio, K. N. Altmann, and F. J. Himpsel, Phys. Rev. B **61**, 10845 (2000).
[89]R. J. Hamers and D. G. Cahill, J. Vac. Sci. Technol. B **9**, 514 (1991).
[90]P. D. C. King, T. D. Veal, A. Schleife, J. Zuniga-Perez, B. Martel, P. H. Jefferson, F. Fuchs, V. Munoz-Sanjose, F. Bechstedt, and C. F. McConville, Phys. Rev. B **79**, 205205 (2009).
[91]W. Göpel, J. Pollmann, I. Ivanov, and B. Reihl, Phys. Rev. B **26**, 3144 (1982).
[92]K. Keem, H. Kim, G. T. Kim, J. S. Lee, B. Min, K. Cho, M. Y. Sung, and S. Kim, Appl. Phys. Lett. **84**, 4376 (2004).
[93]I. Beinik, M. Kratzer, A. Wachauer, L. Wang, Y. P. Piryatinski, G. Brauer, X. Y. Chen, Y. F. Hsu, A. B. Djurisic, and C. Teichert, Beilstein J. Nanotech. **4**, 208 (2013).
[94]K. Siegbahn, Philos. Trans. R. Soc. A **318**, 3 (1986).
[95]W. Göpel, Prog. Surf. Sci. **20**, 9 (1985).
[96]W. Göpel, L. J. Brillson, and C. F. Brucker, J. Vac. Sci. Technol. **17**, 894 (1980).
[97]H. Rupprecht, J. Phys. Chem. Solids **6**, 144 (1958).
[98]S. M. Sze and K. K. Ng, *Physics of Semiconductor Devices*, 3rd ed. (Wiley-Interscience, Hoboken, New Jersey, 2007).
[99]P. S. Xu, Y. M. Sun, C. S. Shi, F. Q. Xu, and H. B. Pan, Nucl. Instrum. Meth. B **199**, 286 (2003).

[100]P. Bonasewicz, W. Hirschwald, and G. Neumann, Phys. Status Solidi A **97**, 593 (1986).

[101]Y. Shapira, S. M. Cox, and D. Lichtman, J. Vac. Sci. Technol. **13**, 334 (1976).

[102]It has been suggested that a similar role may be possible for the metastable singly ionized state, but only at low temperature (Ref. 34).

[103]Under the laser fluence of our experiment, we estimate that the number of un-ionized oxygen vacancies exceeds the concentration of photoionized vacancies by a factor of at least 100.

[104]K. Jacobi, G. Zwicker, and A. Gutmann, Surf. Sci. **141**, 109 (1984).

[105]The difference in dark carrier lifetime values between Fig. 8 (0.6 ms) and Fig. 7(b) (1.2 ms) is a topic for future investigation under more closely controlled conditions. In this case, we believe it could be due to small differences in experimental conditions (timing and partial pressures) in two different experiments; the factor of two then gives an estimate of the amount of variation that could be introduced by the experimental technique.

[106]W. A. Tisdale, K. J. Williams, B. A. Timp, D. J. Norris, E. S. Aydil, and X. Y. Zhu, Science **328**, 1543 (2010).

[107]W. E. Beadle, J. C. C. Tsai, and R. D. Plummer, *Quick Reference Manual for Silicon Integrated Circuit Technology* (Wiley, New York, 1985).

[108]R. M. Tromp, R. J. Hamers, and J. E. Demuth, Science **234**, 304 (1986).

[109]M. Fujita, H. Nagayoshi, and A. Yoshimori, Surf. Sci. **259**, 351 (1991).

[110]W. Mönch, *Semiconductor Surfaces and Interfaces*. (Springer-Verlag, Berlin, New York, 1993).

[111]C. Noguez, A. I. Shkrebtii, and R. Delsole, Surf. Sci. **318**, 342 (1994).